



**STScI** | SPACE TELESCOPE  
SCIENCE INSTITUTE

## JWST TECHNICAL REPORT

Title: NIRISS NRM Phase Calibration: (NIS-016, APT 1508)	Doc #: JWST-STScI-009181, SM-12 Date: 29 September 2025 Rev: -
Authors: Anand Sivaramakrishnan, Kevin Volk, Rachel Cooper, Deepashri Thatte Phone:	Release Date: 8 December 2025

### 1 Abstract

We present the analysis and results of the calibration activity NIS-016 NIRISS NRM Phase Calibration (APT 1508, PI Sivaramakrishnan). NIRISS NRM uses a non-redundant aperture mask, or NRM which in theory should deliver closure phases of zero when observing a point source target (e.g., Sivaramakrishnan et al., 2023). The result of this measurement is sets of closure phase values (one set for each of the F480M, F380M, and F430M filters) describing the mask. F277W data was not collected. These results could be used as inputs for AMI data reduction, to trend AMI stability, or for other calibration purposes such as charge migration studies. These data are also used to measure segment-to-segment pistons as a byproduct of the analysis, and compare intermediate results on fringe phases, fringe amplitudes, and closure phases and closure amplitudes across the three filters.

### 2 Introduction

This activity acquired and analyzed data on gamma Mus (HR 4773, HD 109026), a typical AMI PSF reference star. It is a B5V+A spectroscopic binary. Its WISE W1 and W2 magnitudes are 4.346 and 4.131; these are probably affected by saturation, so the 2MASS Ks magnitude (4.254 +/- 0.015) was used to estimate the NIRISS long wavelength filters' exposure times. The spectral energy distribution of the star does not show a significant excess at these wavelengths, so the magnitude difference between W1 and W2 was not considered to be due to a stellar wind contribution. In case the program needs to be executed again, full temporal coverage is ensured by two other possible targets, HR 2401, HR 8442. Exposure depth was designed to provide a total of  $10^{10}$  photons in each filter, with peak pixel values in an integration staying below the AMI signal limit (30,000 e-) in an integration. If photon noise is the dominant noise source, the desired exposure depth should support almost 10 magnitudes of AMI point source contrast within AMI's [inner and outer working angles](#). (IWA and OWA, respectively). The calibrated data had  $4.7 \times 10^{10}$ ,  $3.0 \times 10^{10}$ , and  $3.0 \times 10^{10}$  photons respectively in F380M, F430M, and F480M filters. These are higher than anticipated, as the NIRISS detector had significantly more sensitivity than expected when these data were acquired.

Operated by the Association of Universities for Research in Astronomy, Inc., for the National Aeronautics and Space Administration under Contract NAS5-03127

Check with the JWST SOCCER Database at: <https://soccer.stsci.edu>

To verify that this is the current version.

The program was executed with the NRM in the Pupil Wheel (PW) and the three AMI medium band filters, F480M, F430M, F380M, in the Filter Wheel (FW) (see Figure 2-1). The exposures commenced on 2022-07-09 at 1:35:50.001 UTC, and ended 2022-07-09 at 03:15:40.029 UTC. The observation had a total duration (charged time) of about 3 hours.

### 3 Observations

Target acquisition was performed using 7 groups per integration in the 64x64 SUBTAAMI subarray, which is contiguous with the AMI 80x80 science [SUB80 subarray](#). Target location (determined on-board as usual, with the centroiding process described in Holfeltz et al., 2015), was followed by a Small Angle Maneuver to POS1 in SUB80 (see [NIRISS AMI Dithers](#) in JDox pages). Table 3-1 lists target information.

**Table 3-1. Target Summary**

Name	RA (Deg)	Dec (Deg)
Gamma Mus	188.11553641747437	-72.1330271643503

Table 3-2 contains parameters pertaining to each uncalibrated data file prior to processing through the JWST data pipeline. CRDS file selection software used CRDS\_VER 12.0.3, with a CRDS context CRDS\_CTX jwst\_1298.pmap. Version 1.17.0 of the JWST pipeline was used. Target acquisition exposures (from the SUBTAAMI subarray) data are not shown or analyzed here. The columns in Table 3-2 are:

- PW – Active element in the Pupil Wheel
- FW – Active element in the Filter Wheel
- NINTS – Number of integrations
- NGROUPS – Number of groups in an integration
- Level1b – Uncalibrated 4-dimensional data file name root

**Table 3-2. Observations in Program 1508**

PW	FW	NINTS	NGROUPS	Level1b FITS file root name
NRM	F380M	4750	3	jw01508001001_03103_00001_nis_uncal
NRM	F430M	4400	5	jw01508001001_03103_00001_nis_uncal
NRM	F480M	4920	5	jw01508001001_03104_00001_nis_uncal

### 4 Pipeline Analysis Steps

The module jwst.pipeline's Detector1Pipeline, Image2Pipeline were used.

Detector1 was run as follows:

```
stepdict = {"ipc": {"skip": True},
            "persistence": {"skip": True},
            "dark_current": {"skip": True}}
Detector1Pipeline.call(fn,
                      steps=stepdict,
                      save_results=True,
                      save_calibrated_ramp = True,
                      output_dir = outdir)
```

Image2 was run with:

```

result2 = Image2Pipeline()
result2.photom.skip = True
result2.resample.skip = True
result2.save_results = True
result2.output_dir = outdir
result2.run(fn)

```

To extract fringe parameters, `mwst.ami`’s `AmiAnalyzeStep`’ `run()` method was run with:

```

analyze = AmiAnalyzeStep()
analyze.save_results = True
analyze.firstfew = None
analyze.usebp = False
analyze.oversample = 5
analyze.run_bpfix = True
analyze.output_dir = outdir
output_model, outputmodelmulti, lgmodel = analyze.run(fn)

```

#### 4.1 Data Processing

Though level 1a, 2a, and 2b pipeline products are available in the Mikulski Archive for Space Telescopes (MAST), the image cube `calints.fits` products that are suitable input for `mwst.Ami_AnalyzeStep3` are not. We therefore reprocessed the exposures through the `Detector1` and `Image2` pipelines (as shown above).

Bad pixels are flagged by the pipeline in the DQ array of each data file, but simply masking these pixels is insufficient for AMI; the bad pixels need to be corrected in the data in order to accurately centroid the image for the image-plane observable extraction step in `mwst.Ami_AnalyzeStep3`. We used stand-alone code that uses the NRM pupil geometry to identify noise in the image and correct pixel values that produce unphysical signal in *complex visibility* space, the so-called *uv-plane*, which is the Fourier space of the detector array. (Kammerer et al. 2019, 2024). A version developed specifically for AMI (and in the pipeline) was used on the `calints` files before extraction of interferometric observables. However, in extracting fringe variables, the default of fitting the corrected bad pixels in this step was turned off, so as to avoid creating additional correlations in the data.

Pipeline-calibrated, custom bad-pixel corrected `calints` FITS files then yielded the interferometric observables. These are a fringe amplitude in degrees, and a fringe visibility—a dimensionless number between 0 and 1—for each baseline between the seven holes in the NRM, i.e., 21 sets of fringe phases and amplitudes. In addition, a total target flux and a constant bias or pedestal background level in the image was also measured. The latter two quantities do not play a role in recovering image morphology. Output from `mwst.Ami_AnalyzeStep3` are two [OIFITS v2](#) format FITS file. One contains observables from each `calints` slice (integration) of the input file, written out to a Multi extension “multi-oi-fits” file, the other is a summary single OIFITS “oi-fits” file containing averages of these quantities. The averaging is over all integrations in the exposure. 3-standard deviation clipped means, standard errors, and covariance matrices are also written out.

However, closure amplitudes (referred to as “quads”, since they are calculated using four baselines at a time) are not included in `mwst.Ami_AnalyzeStep3`’s output files. Quad quantities and statistics for each observation were calculated with custom code that read in each inte-

gration’s fringe observables in the “multi-oi-fits” file. These quad averages were written to local storage for further examination.

Since JWST is far more stable than ground-based telescopes operating at similar wavelengths, the wavefront phase differences between apertures in the mask (pistons) are also saved by `jwst.Ami_AnalyzeStep3`. Each AMI calibration star observation retrieves the segment pistons of JWST. This is unusual in optical & IR interferometry. Such pistons’ temporal trending can measure the stability of the AMI wavefront. A description of our extraction of interferometric variables can be found in [Greenbaum et al., 2015](#), [Sivaramakrishnan et al., 2023](#) and references therein.

Results from the analysis of this program’s interferometric variables is presented in subsections 4.2-4.5 below. These cover:

- Fringe phases and amplitude
- Triple product phases and amplitudes
- Quad phases and amplitude
- Segment pistons
- Comparison of phases and visibilities across filters

Figure 4-1 shows the segment numbering used in this report. Angular quantities are reported in degrees.

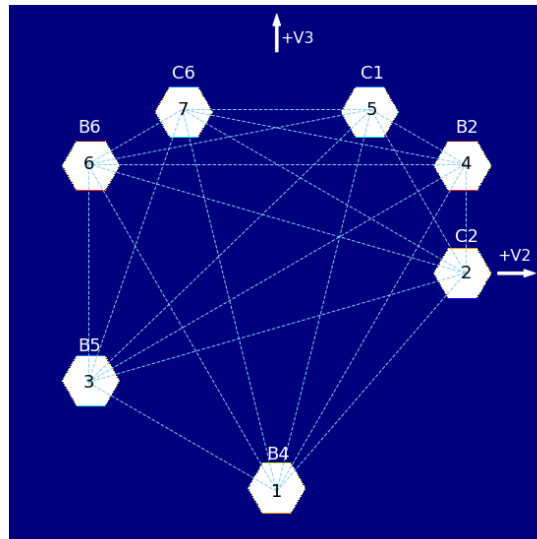


Figure 4-1 NIRISS' NRM in JWST primary mirror (PM) V2-V3 coordinates, with an ideal (distortion-free) projection back to the primary. Seven hexagonal subapertures, 0.80~m flat-to-flat when projected back to V2-V3 space, provide 21 center-to-center baselines with  $l$  lengths between 1.32~m and 5.28~m. Each hole is nominally centered on a 1.32 m flat-to-flat PM segment. Undersized subapertures mitigate against pupil misalignment and shear. Hexagonal holes maximize throughput pupil but tolerate up to 3.8% PM diameter misalignment. Hole locations on only the outer edges maximise long baseline coverage at different orientations while preserving non-redundancy. Shorter baselines also exist between holes, to provide broader fringes that improve coverage of the interferometric uv-plane. The NRM exposes approximately 15% of the JWST primary mirror.

## 4.2 Fringe phase and amplitudes

A fringe is an intensity ripple pattern on the detector. It is created by the interference of light passing between two apertures in the pupil mask. The ripples on the detector are perpendicular to the baseline between two apertures that create them. A fringe is described by a normalized visibility amplitude  $V$  (between 0 and 1) and a fringe phase  $\phi$  (between -180 and 180 degrees). These are combined into a complex fringe visibility as a shorthand. 21 ( $7 \times 6 / 2$ ) ripples are created by the seven holes in the NRM.

Raw complex fringe visibilities are measured here, as a single putatively point-like source was observed. Typically, quantities derived from these raw observables would be used to calibrate a science target's observables.

Fringe amplitudes (the absolute values of fringe complex visibilities) are unity for a monochromatic point source under perfect imaging conditions. They decrease to zero for a uniform brightness source. When the bandpass of detected light is finite, fringe amplitudes decrease with increasing baseline length. Reduced imaging quality also decreases source's fringe amplitudes. JWST imaging at these wavelengths possesses Strehl ratios of  $\sim 94\%$  and higher, so near-unity fringe amplitudes at short baselines are expected (Sivaramakrishnan et al. 2023b). Observed fringe amplitudes, shown in Figure 4-2, range between 0.98 and 0.64. They are measured in these data to an accuracy of  $\sim 10^{-3}$ . Fringe amplitudes provide information on the symmetric component of a target's 2-dimensional sky brightness distribution. There are 21 independent fringe visibilities.

Fringe phases would be zero for a perfect optical system observing an on-axis monochromatic point source. A fringe phase measures the tilt (the displacement of the centroid of the fringe's light distribution) with respect to the telescope pointing (or center of the numerical subarray being analyzed). The fringe phase values by themselves do not contain information on source structure. Given the arbitrariness of telescope pointing (or the phase origin), there are only 20 independent fringe phases (Readhead et al., 1980). These data yield fringe phases within  $\pm 40^\circ$ , with errors of the order of 0.02 (Figure 4-2).

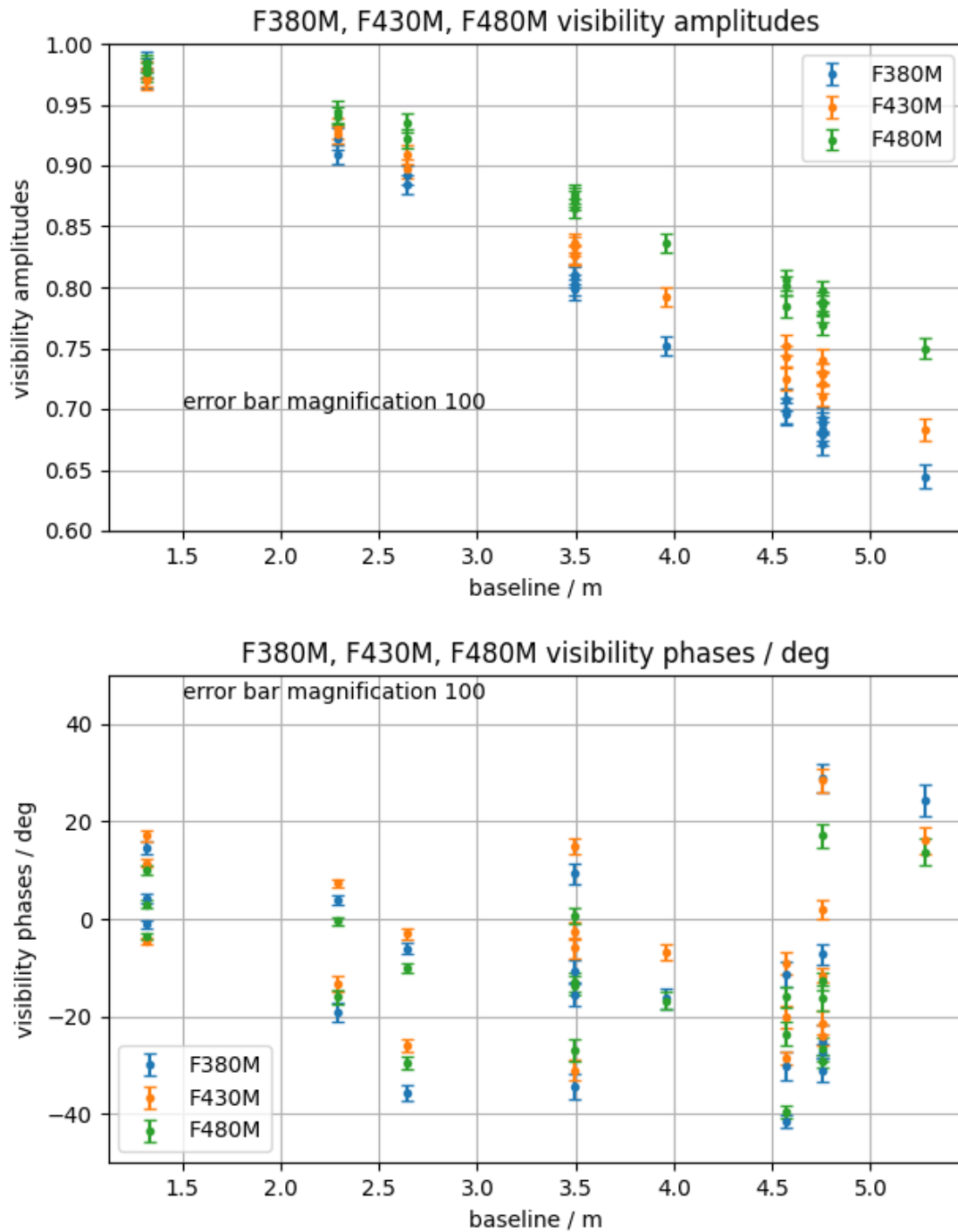


Figure 4-2. Raw fringe complex visibility (VIS) amplitudes and phases for all three filters. Fringe phases measure the tilt (displacement) of the centroid of the light distribution with respect of the telescope pointing (or center of the numerical subarray being analyzed). The top panel shows complex visibility amplitudes versus hole pair baseline length. Visibilities with shorter baselines are close to the perfect monochromatic value, unity, and they drop monotonically with increasing baseline length, to about 0.7 at the longest baselines. Visibility amplitudes are highest for F480M, and lowest to F380M. Error bars are magnified by a factor of 100. The bottom panel shows complex visibility phases (in degrees) versus baseline at length. These phases of distributed around zero with largest deviations of 30 to 40°. Phase error bars are also magnified by a factor of 100.

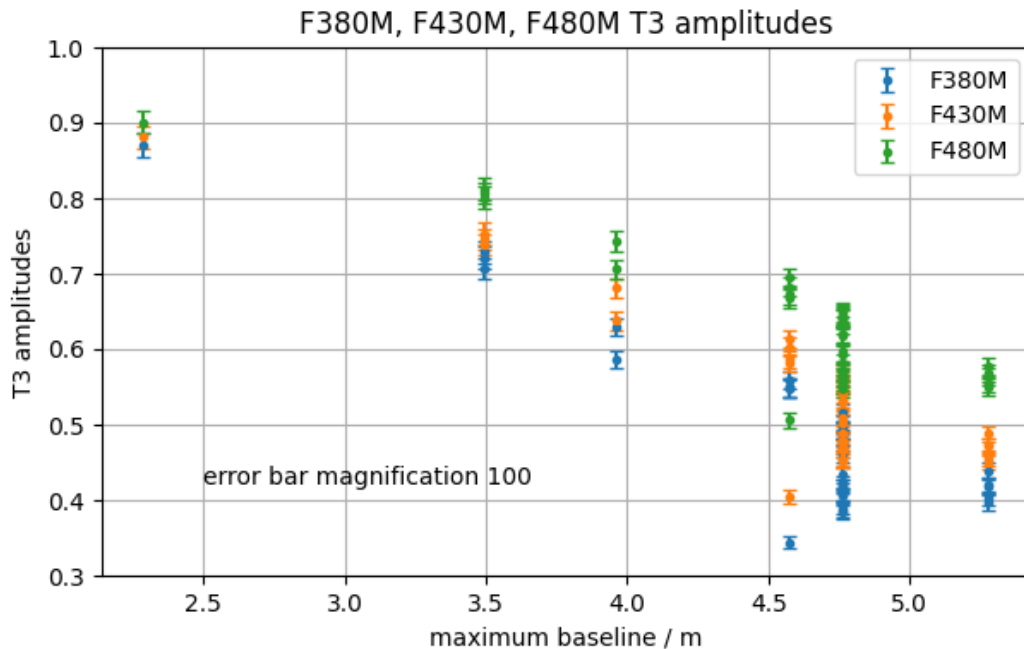
### 4.3 Triple product phases and amplitudes.

A triple product (bispectrum) is the product of the three complex visibilities generated by a triangle of baselines drawn between three apertures in the NRM, taken in order around the triangle so as to maintain consistency in the sign of the phase. 35 ( $7 \times 6 \times 5 / (3 \times 2)$ ) ripples are created by the seven holes in the NRM. Only 15 ( $6 \times 5 / 2$ ) of these are independent ([Readhead et al., 1980](#)).

The phase of the triple product is known as the closure phase. It is insensitive to telescope pointing or target placement within a subarray. Under perfect imaging conditions closure phases are zero for a monochromatic point source, or a source with only radially symmetric structure. Raw closure phases on an isolated reference star (such as this target) contain removable instrumental contributions to observations of other targets, as long as systematics and detector artifacts do not change between observations. Closure phases provide information on the antisymmetric component of the intensity distribution of the target.

These data yield closure phases within  $\pm 1^\circ$ , with errors below  $\sim 0.005^\circ$  (Figure 4-3). If calibration using these closure phases was perfect, the maximum error in calibrated triple product phases would be  $\sim 0.008^\circ$ . That translates to approximately a 7500:1 achievable contrast ratio in the fringes with the largest error, but more typically a 10000:1 (or better) fringe contrast ratio would be supported by most baselines (a rule of thumb is that the contrast ratio is of the order of the closure phase error, measured in radians).

Triple product amplitudes are not typically used in traditional interferometric analyses but are shown for completeness in Figure 4-3.



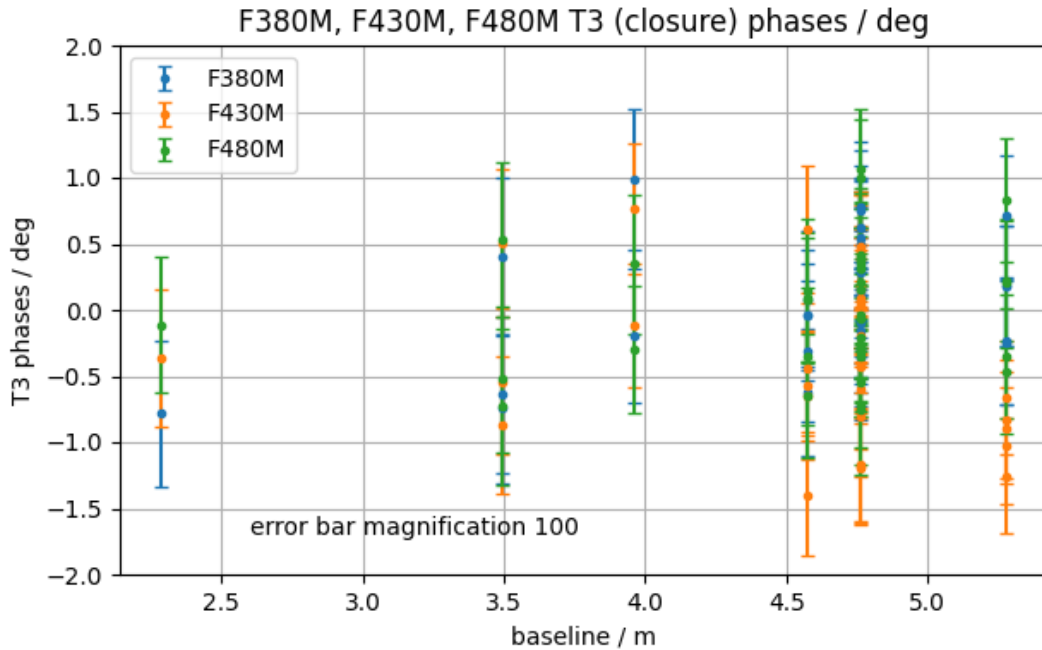


**Figure 4-3. Raw complex triple product (T3) amplitudes and phases for all three filters. Triple product phases, also called closure or bispectrum phases, are ideally zero for a point source or any symmetric light distribution (regardless of telescope pointing or subarray choice). The closure phase values here would be used to subtract instrumental contributions from a science observation's closure phases. That top panel shows the complex triple products amplitudes versus maximum baseline length amongst the triple products' three constituent fringes. Triple product amplitudes fall steadily from 0.9 at the shortest baselines to about 0.5 at the longest maximum baselines. Error bars are magnified by a factor of 100. The bottom panel shows complex triple product phases (in degrees) versus maximum baseline length. Triple product phases are so-called calibratable interferometric observables. They lie within  $1.5^\circ$  of the ideal value of zero (for a point source). Triple product phase error bars are also magnified by a factor of 100.**

#### 4.4 Quad phases and amplitudes.

A quad is the product  $CV_{12} \times CV_{34} / (CV_{13} \times CV_{24})$ , where  $CV_{ij}$  is the complex visibility between apertures  $i$  and  $j$  ( $i \neq j$ ). 35 ( $7 \times 6 \times 5 \times 4 / (4 \times 3 \times 2)$ ) quads are created by the seven holes in the NRM. Only 14 ( $7 \times (7-3) / 2$ ) of these are independent ([Readhead et al., 1980](#)).

The amplitude of the quad is known as the closure amplitude. Closure amplitudes are unity for a monochromatic point source under perfect imaging conditions. Raw closure amplitudes on an isolated reference star (such as this target) contain removable instrumental contributions to observations of other targets, as long as systematics and detector artifacts do not change between observations. Closure amplitudes provide information on the radially symmetric component of the intensity distribution of the target.

These data yield closure amplitudes within 0.5 – 2 (Figure 4-4). These limits are necessarily reciprocals of each other, since the set of all closure amplitudes contains a closure amplitude and its reciprocal. The largest measured closure amplitude error is  $\sim 0.0005$ .

Quad phases are not typically used in traditional interferometric analyses but are shown for completeness in Figure 4-4.

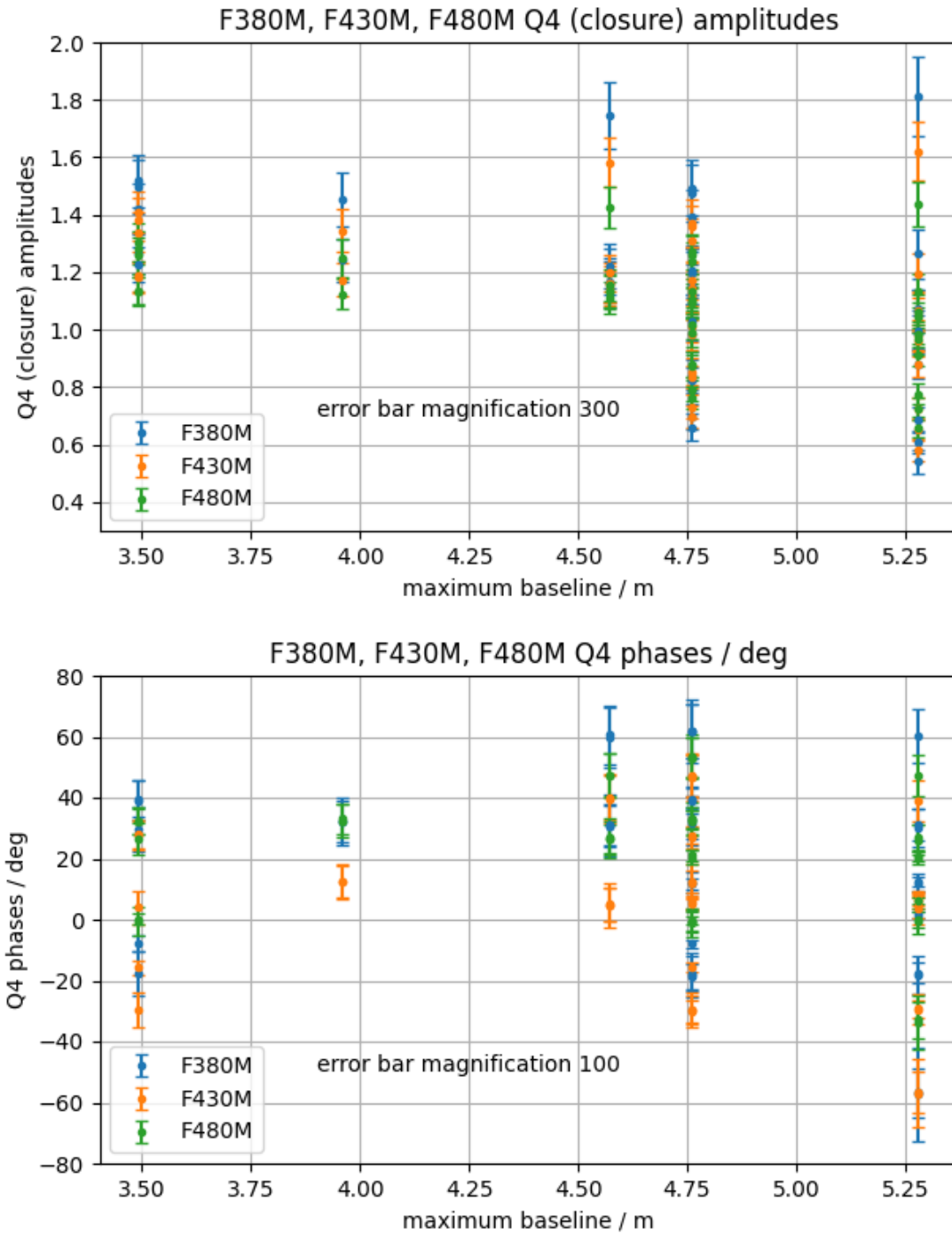


**Figure 4-4. Raw quad amplitudes phases.** Quad amplitudes (closure amplitudes), ideally unity for a point source), are independent of the throughput of each aperture, and are calibratable interferometric observables. The values here would be used to divide those of a science observation to remove instrumental effects. The top panel shows the quad amplitudes versus maximum baseline length amongst the four fringes used to calculate the quad. Quad amplitudes lie between 2 and 0.5 (necessarily reciprocals of each other). Their error bars are magnified by a factor of 300. Quad amplitudes are so-called calibratable observables. The bottom panel shows complex quad phase (in degrees) versus maximum baseline length. These phases lie between +/-80°. Error bars on magnified by a factor of 100.

## 4.5 Segment piston.

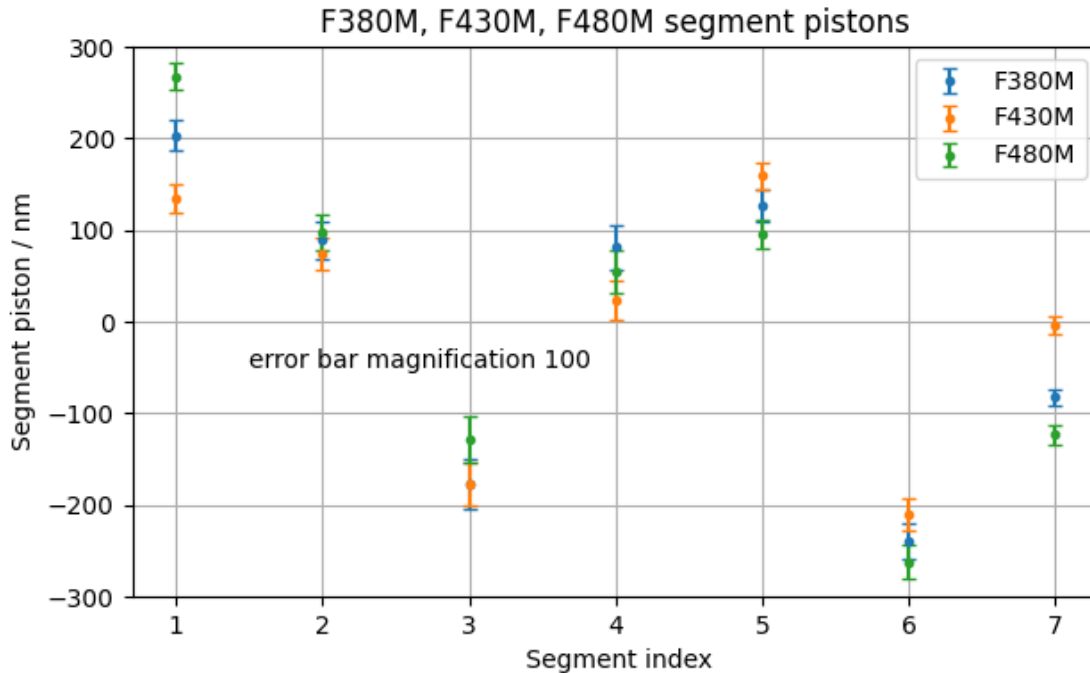


Figure 4-5. Seven segment phases (with zero mean). Pipeline analysis of calibrator star data produces a piston measurement in wavefront phase. These are converted here to OPD (in nanometers) at the filter bandpasses' central wavelengths. They are plotted against segment number (which has no physical interpretation but is merely used to distinguish points in the plot). The analysis produces a set of pistons with zero mean. In theory these data depend on the optical system only if the object is a point source. These pistons lie within 300 nm of zero. Error bars are magnified by a factor of 100.

Differences in the sets of (the 7 zero mean) pupil phases between all pairs of calibrators have approximately 17 nm RMS optical path delay (OPD). NIRCAM immediately post-commissioning wavefront error was about 50nm RMS, which is a Strehl ratio well above 80% at 2 microns. These segment level pistons by themselves reduce the Strehl ratio by considerably less than 1%, by the Maréchal approximation (A. Maréchal, 1947).

## 4.6 Comparison of observables' phases and amplitudes across filters.

As indicated in section 4.5 above, a fringe phase  $\phi$  (in radians) can in principle be translated to an OPD (in meters) using the relation  $OPD = \lambda\phi/2\pi$  (where  $\lambda$  is the effective central wavelength of the bandpass, taking into account the spectrum of the source and the filter bandpass). The same is true of closure and quad phases, since they are linear combinations of fringe phases. It follows then, that these phases, converted to OPD in meters, should be the same if the wavefront error is the same for all filters.

Finite filter band pass, chromatic detector sensitivity, and changes in source spectral shape can complicate this relationship. It is useful to examine the differences in OPDs of each fringe across filters. Since closure phases for this calibrator star are ideally zero, it is also interesting to compare them across filters. In Figure 4-6 we compare phases in the F380M and F430M with those of F480M. We use F480M as the reference filter because it has the best image plane sampling,

so it probably provides the most reliable measurements. We use the central wavelengths in the data files headers.

Closure phases (T3 phases) do not correlate with each other across filters as well as the fringe phases do. However, these raw closure phases are tightly clustered around ideal value of zero. This makes the lower correlation of closure phases across filters less problematic, since the correlations are likely dominated by random, mostly photon-noise, errors.

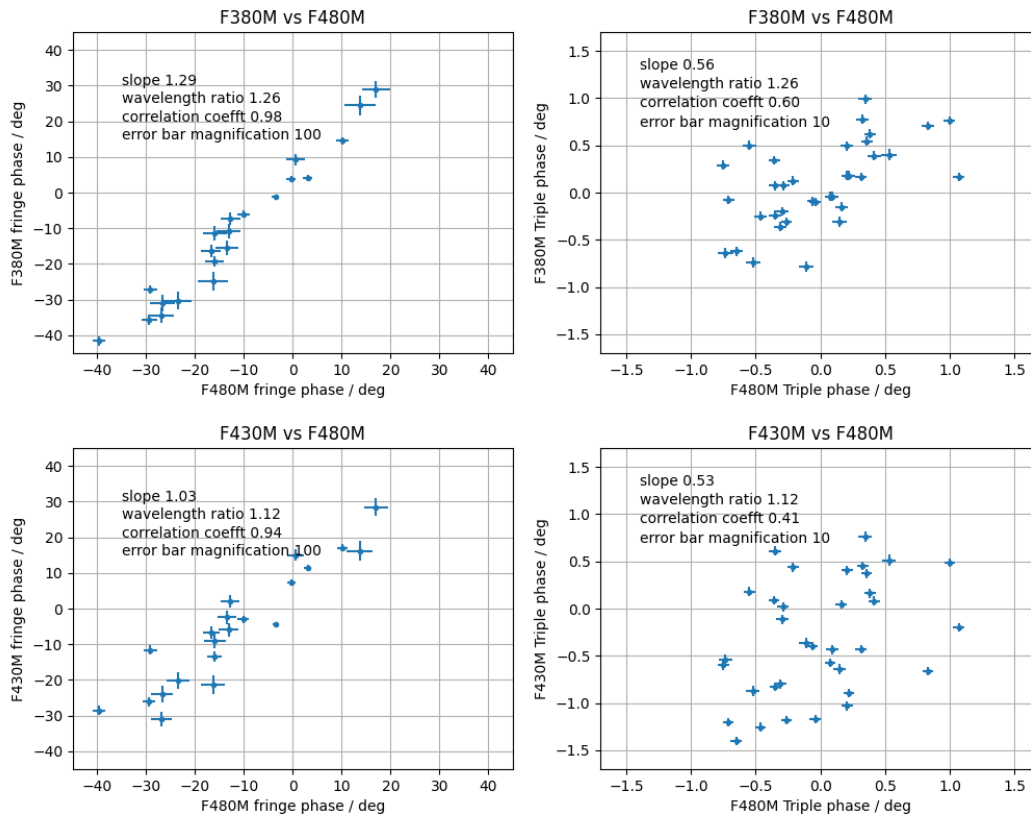


**Figure 4-6. Visibility and T3 phase consistency across filters.** For a given set of baselines or triangles, phases should vary in inverse proportion to the filter's central wavelength. In the top two panels, F380M and F430M fringe and T3 (closure) phases are plotted against those of F480M. Fringe phases have a 0.98 correlation coefficient over the range  $-40^\circ$  to  $30^\circ$ . T3 phases range over  $\pm 1^\circ$ , with a correlation coefficient of 0.6. The fitted linear slope (1.29) is close to the wavelength ratio (1.26) between the filters' central wavelengths. Tighter T3 phase clustering likely results in small random noises causing a lower correlation (0.60) of these T3 phases, which in the ideal case, should be exactly 0. The bottom two panels compare F430M and F480M fringe and T3 phases similarly. The fringe phase correlation coefficient is lower (0.94), and the fitted slope (1.03) is further from wavelength ratio (1.12) in this case. T3 phases also show a lower correlation (0.41), with the spread of phases between  $-1.5^\circ$  and  $1^\circ$ . The lower correlation between these two filters' T3 values is again likely due to residual random noise. This may indicate that the wavefront error differences between the F380M and F480M filters is larger than the differences between F430M and F480M filters' wavefront errors.

Linear correlation coefficients are shown in each plot. Correlation between F380M and F480M fringe phases (0.98) is better than the correlation between F430M and F480M fringe phases (0.94). This suggests that wavefront error in 430M is the odd one out, with the wavefront error in F380M being closer to that in F480M.

Fringe amplitudes have a less meaningful comparison in the broadband case but we present them consistency in Figure 4-7. The correlation between fringe amplitudes in all three filters is almost perfect. This is not surprising, since fringe amplitude depends on segment throughout, which is not expected to vary much in the 3-5 micron wavelength range.

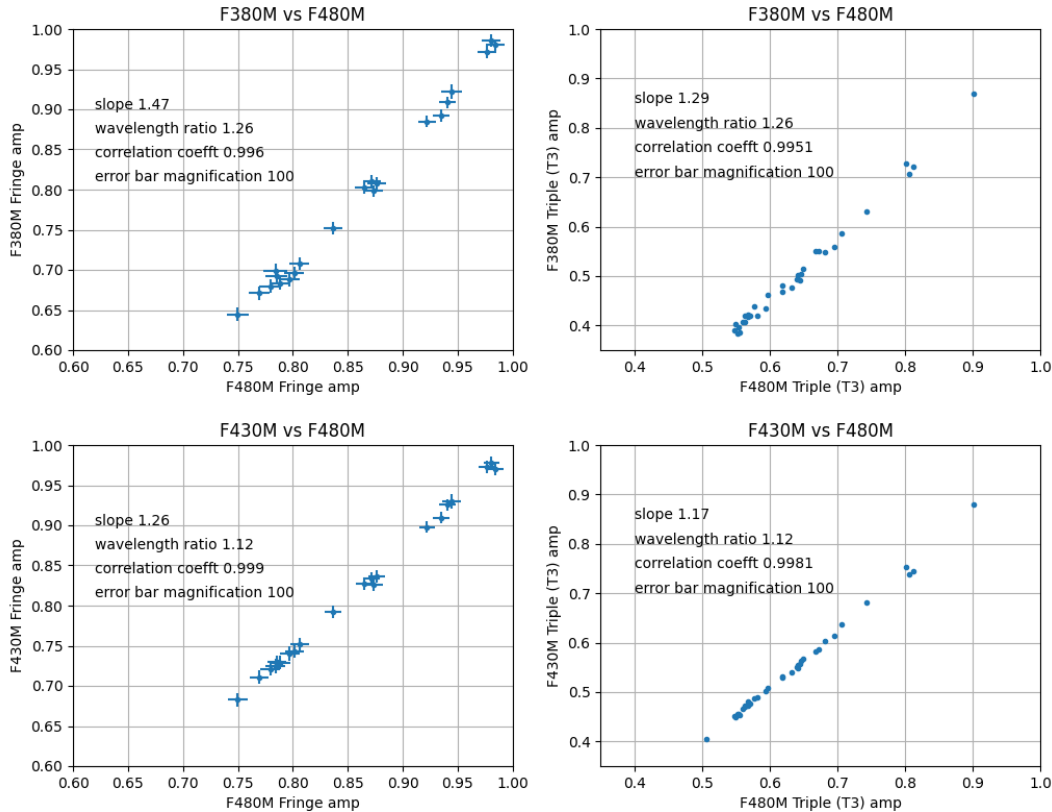


**Figure 4-7. Visibility and T3 amplitude consistency across filters. High correlations (above 0.99) in both comparisons (F380M vs F480M in the two panels, and F430M vs. F480M in the bottom two panels) confirms extreme temporal image stability during the visit. Non-unity slopes in the linear fits may be purely due to bandpass shape effects being different in all three filters.**

Since the quads were calculated with post-pipeline processing, they are presented separately here (Figure 4-8). Quad amplitudes, which are the closure phases of the observation, are highly correlated between filters. Quad phases are almost as tightly correlated, which was unexpected. Correlations between the F380M filter's quad properties and F480M's were slightly lower than the corresponding correlations between F430M quads and F480M's, a qualitative change from closure phase correlations across filters. Reasons for this reversal unclear - the more interesting behavior is the extremely tight correlation across filters for the complex quantity. It is not immediately obvious what this means in terms of science performance or wavefront error

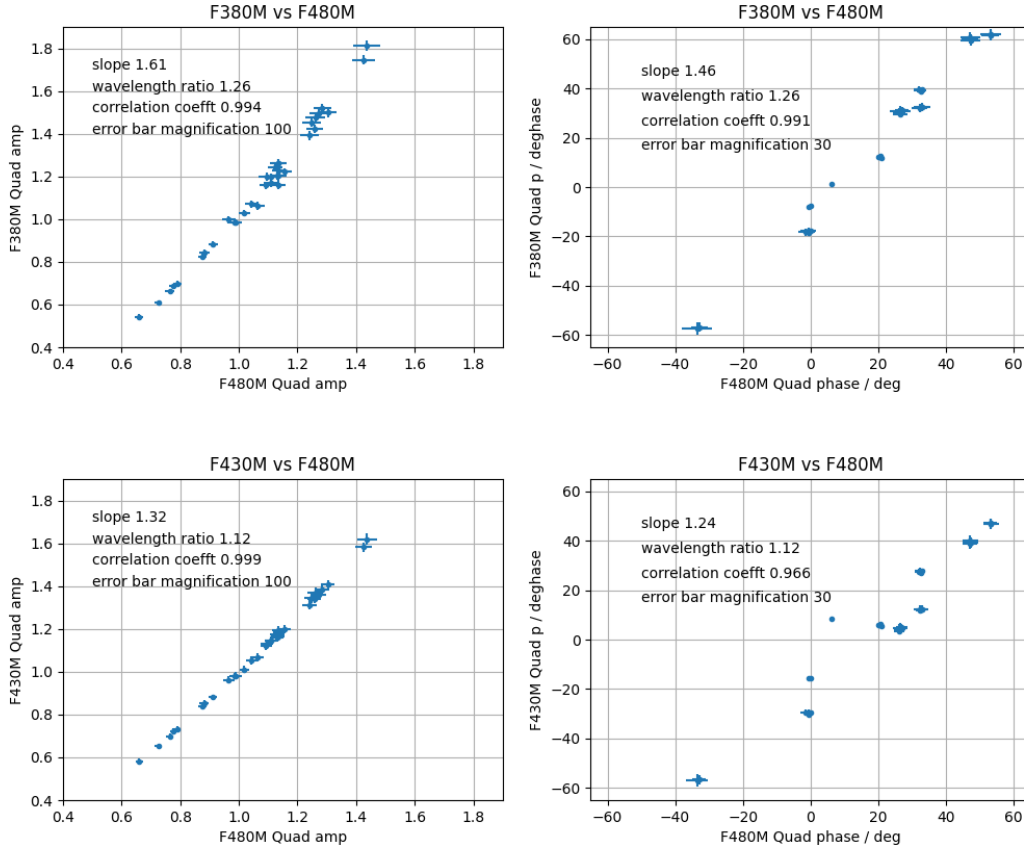


**Figure 4-8. Raw quad amplitudes phases.** Quad amplitudes (closure amplitudes, ideally unity for a point source), are independent of the throughput of each aperture, so are calibratable interferometric observables. The values here would be used to divide those of a science observation to remove instrumental effects. The top panel shows the quad amplitudes versus maximum baseline length amongst the four fringes used to calculate the quad. Quad amplitudes lie between 2 and 0.5, which are necessarily reciprocals of each other. Their error bars are magnified by a factor of 300. The bottom panel shows complex quad phase (in degrees) versus maximum baseline length. The phases lie between  $\pm 80^\circ$ . Error bars on magnified by a factor of 100.

## 5 Summary and conclusion.

The main difference between “calibratable” ground based non-redundant masking observables and those of AMI is that AMI’s space-based observables show orders of magnitude more stability than quantities derived from visibility amplitudes. The stability and small scatter of AMI observables, even those that do not calibrate well in ground data, match AMI performance predictions made before launch ([Sivaramakrishnan, A. et al., SPIE 2012](#)). This amply confirms internal stability of JWST during a single pointing.

At the photon noise limit, the binary point source contrast achievable at, and just outside, the inner working angle of AMI is approximately the inverse of the closure phase measurement error (in radians). Since random errors in AMI observables are dominated by photon noise at our exposure depth ( $\sim 10^{10}$  photons in each filter), we only consider the photon noise contribution to the measurement error (Equation 22 of [Ireland 2013](#)) for a seven-hole mask. Assuming fringe visibilities are of the order of unity, this yields closure phase errors  $\sim 100 / \text{sqrt}(\text{number of photons})$ . Measured closure phase errors (Table 5.1) are  $\sim 0.005$  degrees ( $9e-5$  radian). The contrast limit set by measurement error on this single star observation is then of the order of  $10^4$  (10 magni-

tudes). The Ireland estimate applied to the number of photons detected predicts an achievable contrast of over 11 magnitudes, but the most demanding science drivers that motivated adding the AMI mode to NIRISS required 10 magnitudes of binary point source contrast.

In practice, systematics are introduced because a science target and its calibrator are performed in distinct observations. These systematics currently limit AMI’s achievable contrast ratio to ~8 magnitudes. Using two nights of Keck time, observing HR8799 and 8 calibrator stars, [Hinkley et al., ApJL 2011](#) achieved a contrast limit of 8 magnitudes at best. Should systematic errors be properly accounted for, AMI’s binary contrast limit could approach 10 magnitudes given the image stability demonstrated here.

**Table 5-1. Triple product T3 mean amplitude and phase errors for the AMI medium band filters. The measurement error of these triple product closure phases, ~9e-5 radians, is similar in all three filters. Closure phases are traditionally well-calibrated observables in ground-based masking.**

Filter	Amplitude error	Phase error / deg
F380M	0.00011	0.00482
F430M	0.00011	0.00482
F480M	0.00011	0.00482

**Table 5-2. Quad Q4 mean amplitude and phase errors for the AMI medium band filters. The measurement error of these are similar in all three filters. Closure amplitudes, though in principle calibratable, are traditionally poorly-calibrated observables in ground-based masking because of atmospheric transparency variations (scintillation).**

Filter	Amplitude error	Phase error / deg
F380M	0.00025	0.06412
F430M	0.00025	0.06563
F480M	0.00018	0.04452

## 6 References

[Gardner, J. P. et al. PASP 2023](#)

[Greenbaum et al., ApJ 2015](#)

[Hinkley et al., ApJL 2011](#)

[Ireland, M. J., MNRAS 2013](#)

Maréchal, André, "Etude des effets combinés de la diffraction et des aberrations géométriques sur l'image d'un point lumineux," Rev.d'Opt. 26, 257-277, 1947.

[Readhead, A. C. S. et al., Nature, 1980](#)

[Sivaramakrishnan, A. et al., SPIE 2012](#)

[Sivaramakrishnan et al., PASP, 2023a](#)

Sivaramakrishnan et al., 2023b, JWST Technical Report JWST-STScI-008334, SM-12

## 7 Appendix: Tables of observables from pipeline and post-processing data

Fringe visibilities, triple products (T3, or bispectra), and quads (Q4) values and standard errors from the JWST pipeline for AMI, and post-processing pipeline oifits output to calculate quad quantities. One table per filter is included. All possible baseline combinations are included, so the triple product and quad quantities are not independent sets. Amplitudes (“amp”) and phases

(“phi”) of complex quantities are presented, along with baseline vectors (u, [v], [w]) and [maximum] baseline lengths (bl) as appropriate, for visibilities and triple products. With hitherto ground-based-only aperture masking data, intuition on quads and their baseline geometries is lacking. We therefore do not present them here.

**Table 7-1. F380M complex visibilities.**

	amp	amperr	phi/deg	phierr/deg	u/m	v/m	bl/m
<b>0</b>	0.810493	0.000082	-10.863539	0.024835	-1.862175	2.954508	3.492394
<b>1</b>	0.885027	0.000078	-35.624408	0.016050	-1.927127	-1.804382	2.640002
<b>2</b>	0.695647	0.000092	-11.359529	0.025077	-3.125276	3.337883	4.572616
<b>3</b>	0.683764	0.000093	-7.284495	0.020971	-4.088841	2.435687	4.759327
<b>4</b>	0.707296	0.000091	-41.608097	0.013222	-4.453328	-1.037632	4.572616
<b>5</b>	0.688177	0.000090	-27.147687	0.013545	-4.752864	0.247939	4.759327
<b>6</b>	0.671294	0.000093	-24.856957	0.030048	-0.064951	-4.758890	4.759333
<b>7</b>	0.971271	0.000083	-1.118691	0.007308	-1.263101	0.383375	1.320000
<b>8</b>	0.908649	0.000077	3.866796	0.008945	-2.226666	-0.518821	2.286310
<b>9</b>	0.679690	0.000096	-31.048347	0.025464	-2.591153	-3.992140	4.759333
<b>10</b>	0.752013	0.000083	-16.363029	0.020098	-2.890689	-2.706569	3.959999
<b>11</b>	0.644422	0.000098	24.446115	0.031905	-1.198150	5.142265	5.280005
<b>12</b>	0.691723	0.000096	28.885647	0.029239	-2.161714	4.240069	4.759327
<b>13</b>	0.892285	0.000078	-6.024434	0.012507	-2.526202	0.766750	2.640000
<b>14</b>	0.808046	0.000083	9.253320	0.019581	-2.825738	2.052321	3.492394
<b>15</b>	0.985275	0.000084	4.200527	0.009417	-0.963565	-0.902196	1.320006
<b>16</b>	0.698973	0.000106	-30.289095	0.028654	-1.328052	-4.375515	4.572620
<b>17</b>	0.802425	0.000084	-15.441854	0.023493	-1.627588	-3.089944	3.492391
<b>18</b>	0.798183	0.000086	-34.416689	0.026245	-0.364487	-3.473319	3.492391
<b>19</b>	0.921697	0.000091	-19.240910	0.019532	-0.664023	-2.187748	2.286300
<b>20</b>	0.980183	0.000083	14.535050	0.012791	-0.299536	1.285571	1.320006

Table 7-2: F430M complex visibilities.

	amp	amperr	phi/deg	phierr/deg	u/m	v/m	bl/m
0.000000	0.834252	0.000076	-5.928056	0.020663	-1.862176	2.954507	3.492394
1.000000	0.897546	0.000074	-26.069202	0.013160	-1.927126	-1.804383	2.640002
2.000000	0.743189	0.000084	-9.031328	0.022204	-3.125277	3.337882	4.572616
3.000000	0.728734	0.000092	1.990911	0.019208	-4.088841	2.435686	4.759327
4.000000	0.751989	0.000084	-28.618885	0.013374	-4.453328	-1.037633	4.572616
5.000000	0.740286	0.000090	-11.554006	0.013937	-4.752864	0.247938	4.759327
6.000000	0.710915	0.000085	-21.312343	0.025135	-0.064951	-4.758890	4.759333
7.000000	0.972667	0.000077	-4.506001	0.006797	-1.263101	0.383375	1.320000
8.000000	0.925389	0.000074	7.318811	0.008623	-2.226666	-0.518821	2.286310
9.000000	0.720938	0.000086	-23.868023	0.021604	-2.591152	-3.992140	4.759333
10.000000	0.791963	0.000079	-6.826911	0.017103	-2.890688	-2.706569	3.959999
11.000000	0.683016	0.000090	16.145775	0.026848	-1.198150	5.142265	5.280005
12.000000	0.729611	0.000085	28.431203	0.024945	-2.161715	4.240069	4.759327
13.000000	0.909389	0.000076	-2.985010	0.011543	-2.526202	0.766750	2.640000
14.000000	0.836503	0.000078	14.966512	0.017177	-2.825738	2.052321	3.492394
15.000000	0.978510	0.000074	11.459144	0.007732	-0.963565	-0.902196	1.320006
16.000000	0.724702	0.000093	-20.161888	0.023461	-1.328051	-4.375515	4.572620
17.000000	0.827670	0.000077	-2.435510	0.019279	-1.627587	-3.089944	3.492391
18.000000	0.826158	0.000078	-31.008753	0.021441	-0.364487	-3.473319	3.492391
19.000000	0.930160	0.000085	-13.383964	0.015610	-0.664023	-2.187748	2.286300
20.000000	0.970116	0.000074	17.082969	0.010239	-0.299536	1.285571	1.320006

Table 7-3: F480M complex visibilities.

	amp	amperr	phi/deg	phierr/deg	u/m	v/m	bl/m
0.000000	0.871741	0.000076	-13.130487	0.019516	-1.862176	2.954507	3.492394
1.000000	0.922124	0.000072	-29.441135	0.013564	-1.927126	-1.804383	2.640002
2.000000	0.801224	0.000079	-15.981620	0.021035	-3.125277	3.337882	4.572616
3.000000	0.788212	0.000083	-12.752189	0.017581	-4.088842	2.435686	4.759327
4.000000	0.805943	0.000079	-39.640969	0.013207	-4.453328	-1.037633	4.572616
5.000000	0.797067	0.000085	-29.151355	0.012685	-4.752864	0.247938	4.759327
6.000000	0.769326	0.000083	-16.350468	0.025813	-0.064950	-4.758890	4.759333
7.000000	0.976576	0.000076	-3.503130	0.005793	-1.263101	0.383375	1.320000
8.000000	0.940656	0.000074	-0.371866	0.008041	-2.226665	-0.518821	2.286310
9.000000	0.779343	0.000083	-26.774670	0.022926	-2.591152	-3.992140	4.759333
10.000000	0.836480	0.000077	-16.733184	0.017817	-2.890688	-2.706569	3.959999
11.000000	0.749706	0.000085	13.679234	0.027356	-1.198151	5.142265	5.280005
12.000000	0.785093	0.000081	17.048261	0.024215	-2.161715	4.240069	4.759327
13.000000	0.935067	0.000074	-10.110082	0.010083	-2.526202	0.766750	2.640000
14.000000	0.876514	0.000076	0.616042	0.015627	-2.825738	2.052321	3.492394
15.000000	0.980672	0.000076	3.019144	0.007607	-0.963565	-0.902196	1.320006
16.000000	0.784113	0.000093	-23.582061	0.024574	-1.328051	-4.375515	4.572620
17.000000	0.864835	0.000076	-13.526455	0.019589	-1.627587	-3.089944	3.492391
18.000000	0.873696	0.000076	-26.951536	0.021552	-0.364486	-3.473319	3.492391
19.000000	0.944525	0.000092	-16.015521	0.015412	-0.664023	-2.187748	2.286300
20.000000	0.984094	0.000073	10.202484	0.009727	-0.299536	1.285571	1.320006

Table 7-4. F380M triple products (bispectra).

	amp	amperr	phi/deg	phierr.	u/m	v/m	w/m	maxbl/m
0.00000	0.48152	0.00010	-0.09609	0.00465	-1.86218	-0.06495	1.92713	4.75933
1.00000	0.54762	0.00011	-0.62270	0.00477	-1.86218	-1.26310	3.12528	4.57262
2.00000	0.50356	0.00011	0.28775	0.00489	-1.86218	-2.22667	4.08884	4.75933
3.00000	0.38964	0.00009	-0.30379	0.00418	-1.86218	-2.59115	4.45333	4.75933
4.00000	0.41944	0.00009	-0.07888	0.00444	-1.86218	-2.89069	4.75286	4.75933
5.00000	0.39675	0.00009	0.18124	0.00449	-1.92713	-1.19815	3.12528	5.28001
6.00000	0.41860	0.00010	0.54573	0.00448	-1.92713	-2.16171	4.08884	4.75933
7.00000	0.55855	0.00011	-0.04074	0.00494	-1.92713	-2.52620	4.45333	4.57262
8.00000	0.49214	0.00010	0.77660	0.00494	-1.92713	-2.82574	4.75286	4.75933
9.00000	0.46865	0.00011	0.12549	0.00472	-3.12528	-0.96356	4.08884	4.75933
10.00000	0.34391	0.00008	-0.04053	0.00394	-3.12528	-1.32805	4.45333	4.57262
11.00000	0.38414	0.00009	0.34630	0.00426	-3.12528	-1.62759	4.75286	4.75933
12.00000	0.38602	0.00009	-0.09309	0.00407	-4.08884	-0.36449	4.45333	4.75933
13.00000	0.43370	0.00010	0.62228	0.00468	-4.08884	-0.66402	4.75286	4.75933
14.00000	0.47710	0.00011	0.07464	0.00474	-4.45333	-0.29954	4.75286	4.75933
15.00000	0.42017	0.00010	0.70785	0.00464	-0.06495	-1.19815	1.26310	5.28001
16.00000	0.42193	0.00009	0.16189	0.00446	-0.06495	-2.16171	2.22667	4.75933
17.00000	0.40712	0.00010	0.16696	0.00459	-0.06495	-2.52620	2.59115	4.75933
18.00000	0.40792	0.00009	0.75939	0.00444	-0.06495	-2.82574	2.89069	4.75933
19.00000	0.86955	0.00016	-0.78496	0.00553	-1.26310	-0.96356	2.22667	2.28631
20.00000	0.46144	0.00011	-0.35944	0.00478	-1.26310	-1.32805	2.59115	4.75933
21.00000	0.58610	0.00012	-0.19752	0.00503	-1.26310	-1.62759	2.89069	3.96000
22.00000	0.49296	0.00011	0.49845	0.00501	-2.22667	-0.36449	2.59115	4.75933
23.00000	0.62981	0.00012	0.98892	0.00529	-2.22667	-0.66402	2.89069	3.96000
24.00000	0.50101	0.00011	-0.15027	0.00479	-2.59115	-0.29954	2.89069	4.75933
25.00000	0.43920	0.00011	-0.23901	0.00474	-1.19815	-0.96356	2.16171	5.28001
26.00000	0.40192	0.00010	0.18145	0.00460	-1.19815	-1.32805	2.52620	5.28001
27.00000	0.41784	0.00009	-0.24906	0.00465	-1.19815	-1.62759	2.82574	5.28001
28.00000	0.49265	0.00010	0.49339	0.00485	-2.16171	-0.36449	2.52620	4.75933
29.00000	0.51518	0.00011	0.39142	0.00503	-2.16171	-0.66402	2.82574	4.75933
30.00000	0.70672	0.00014	-0.74270	0.00564	-2.52620	-0.29954	2.82574	3.49239
31.00000	0.54969	0.00012	0.07293	0.00521	-0.96356	-0.36449	1.32805	4.57262
32.00000	0.72870	0.00015	0.40147	0.00594	-0.96356	-0.66402	1.62759	3.49239
33.00000	0.54976	0.00013	-0.31219	0.00532	-1.32805	-0.29954	1.62759	4.57262
34.00000	0.72110	0.00015	-0.64073	0.00588	-0.36449	-0.29954	0.66402	3.49239

**Table 7-5. F430M triple products (bispectra).**

	amp	amperr	phi/deg	phierr.	u/m	v/m	w/m	maxbl/m
0.00000	0.53232	0.00010	-1.17120	0.00435	-1.86218	-0.06495	1.92713	4.75933
1.00000	0.60306	0.00012	-1.40273	0.00451	-1.86218	-1.26310	3.12528	4.57262
2.00000	0.56259	0.00012	-0.60016	0.00456	-1.86218	-2.22667	4.08884	4.75933
3.00000	0.45228	0.00010	-1.17719	0.00418	-1.86218	-2.59115	4.45333	4.75933
4.00000	0.48910	0.00010	-1.20096	0.00426	-1.86218	-2.89069	4.75286	4.75933
5.00000	0.45560	0.00010	-0.89210	0.00422	-1.92713	-1.19815	3.12528	5.28001
6.00000	0.47722	0.00010	0.37109	0.00415	-1.92713	-2.16171	4.08884	4.75933
7.00000	0.61379	0.00012	-0.43533	0.00481	-1.92713	-2.52620	4.45333	4.57262
8.00000	0.55581	0.00011	0.45132	0.00440	-1.92713	-2.82574	4.75286	4.75933
9.00000	0.52995	0.00011	0.43690	0.00432	-3.12528	-0.96356	4.08884	4.75933
10.00000	0.40501	0.00009	-0.57433	0.00411	-3.12528	-1.32805	4.45333	4.57262
11.00000	0.45536	0.00010	0.08717	0.00413	-3.12528	-1.62759	4.75286	4.75933
12.00000	0.45273	0.00010	-0.39896	0.00424	-4.08884	-0.36449	4.45333	4.75933
13.00000	0.50180	0.00011	0.16095	0.00445	-4.08884	-0.66402	4.75286	4.75933
14.00000	0.54005	0.00011	0.01809	0.00442	-4.45333	-0.29954	4.75286	4.75933
15.00000	0.47229	0.00011	-0.66057	0.00430	-0.06495	-1.19815	1.26310	5.28001
16.00000	0.47999	0.00010	-0.19995	0.00424	-0.06495	-2.16171	2.22667	4.75933
17.00000	0.46608	0.00010	-0.42933	0.00428	-0.06495	-2.52620	2.59115	4.75933
18.00000	0.47097	0.00010	0.48108	0.00420	-0.06495	-2.82574	2.89069	4.75933
19.00000	0.88075	0.00015	-0.36567	0.00520	-1.26310	-0.96356	2.22667	2.28631
20.00000	0.50818	0.00011	-0.79987	0.00461	-1.26310	-1.32805	2.59115	4.75933
21.00000	0.63757	0.00012	-0.11460	0.00470	-1.26310	-1.62759	2.89069	3.96000
22.00000	0.55117	0.00011	0.17808	0.00459	-2.22667	-0.36449	2.59115	4.75933
23.00000	0.68169	0.00013	0.76176	0.00494	-2.22667	-0.66402	2.89069	3.96000
24.00000	0.55389	0.00011	0.04186	0.00447	-2.59115	-0.29954	2.89069	4.75933
25.00000	0.48763	0.00011	-0.82629	0.00446	-1.19815	-0.96356	2.16171	5.28001
26.00000	0.45013	0.00010	-1.03110	0.00442	-1.19815	-1.32805	2.52620	5.28001
27.00000	0.47289	0.00010	-1.25625	0.00438	-1.19815	-1.62759	2.82574	5.28001
28.00000	0.54816	0.00011	0.40746	0.00459	-2.16171	-0.36449	2.52620	4.75933
29.00000	0.56770	0.00012	0.08073	0.00470	-2.16171	-0.66402	2.82574	4.75933
30.00000	0.73797	0.00013	-0.86855	0.00520	-2.52620	-0.29954	2.82574	3.49239
31.00000	0.58585	0.00012	0.61228	0.00483	-0.96356	-0.36449	1.32805	4.57262
32.00000	0.75332	0.00014	0.51069	0.00557	-0.96356	-0.66402	1.62759	3.49239
33.00000	0.58189	0.00012	-0.64341	0.00491	-1.32805	-0.29954	1.62759	4.57262
34.00000	0.74549	0.00014	-0.54182	0.00549	-0.36449	-0.29954	0.66402	3.49239

**Table 7-6. F480M triple products (bispectra).**

	amp	amperr	phi/deg	phierr.	u/m	v/m	w/m	maxbl/m
0.00000	0.61843	0.00011	-0.03982	0.00463	-1.86218	-0.06495	1.92713	4.75933
1.00000	0.68210	0.00012	-0.65200	0.00471	-1.86218	-1.26310	3.12528	4.57262
2.00000	0.64634	0.00012	-0.75016	0.00490	-1.86218	-2.22667	4.08884	4.75933
3.00000	0.54755	0.00011	-0.26419	0.00443	-1.86218	-2.59115	4.45333	4.75933
4.00000	0.58122	0.00011	-0.71231	0.00461	-1.86218	-2.89069	4.75286	4.75933
5.00000	0.55390	0.00011	0.21972	0.00457	-1.92713	-1.19815	3.12528	5.28001
6.00000	0.57063	0.00011	0.35931	0.00458	-1.92713	-2.16172	4.08884	4.75933
7.00000	0.69492	0.00012	0.08975	0.00497	-1.92713	-2.52620	4.45333	4.57262
8.00000	0.64423	0.00012	0.32626	0.00482	-1.92713	-2.82574	4.75286	4.75933
9.00000	0.61933	0.00012	-0.21029	0.00481	-3.12528	-0.96356	4.08884	4.75933
10.00000	0.50633	0.00010	0.07729	0.00464	-3.12528	-1.32805	4.45333	4.57262
11.00000	0.55231	0.00011	-0.35672	0.00446	-3.12528	-1.62759	4.75286	4.75933
12.00000	0.55502	0.00011	-0.06276	0.00452	-4.08884	-0.36449	4.45333	4.75933
13.00000	0.59341	0.00012	0.38365	0.00495	-4.08884	-0.66402	4.75286	4.75933
14.00000	0.63217	0.00012	-0.28713	0.00483	-4.45333	-0.29954	4.75286	4.75933
15.00000	0.56326	0.00012	0.83190	0.00464	-0.06495	-1.19815	1.26310	5.28001
16.00000	0.56815	0.00011	1.06966	0.00452	-0.06495	-2.16172	2.22667	4.75933
17.00000	0.56064	0.00011	0.31412	0.00454	-0.06495	-2.52620	2.59115	4.75933
18.00000	0.56406	0.00011	0.99876	0.00443	-0.06495	-2.82574	2.89069	4.75933
19.00000	0.90087	0.00015	-0.11212	0.00514	-1.26310	-0.96356	2.22667	2.28631
20.00000	0.59678	0.00012	-0.31052	0.00498	-1.26310	-1.32805	2.59115	4.75933
21.00000	0.70647	0.00013	-0.29640	0.00483	-1.26310	-1.62759	2.89069	3.96000
22.00000	0.64050	0.00012	-0.54873	0.00486	-2.22667	-0.36449	2.59115	4.75933
23.00000	0.74319	0.00014	0.34580	0.00524	-2.22667	-0.66402	2.89069	3.96000
24.00000	0.64154	0.00012	0.16100	0.00468	-2.59115	-0.29954	2.89069	4.75933
25.00000	0.57721	0.00012	-0.34988	0.00470	-1.19815	-0.96356	2.16172	5.28001
26.00000	0.54968	0.00011	0.20726	0.00488	-1.19815	-1.32805	2.52620	5.28001
27.00000	0.56831	0.00011	-0.46326	0.00477	-1.19815	-1.62759	2.82574	5.28001
28.00000	0.64139	0.00012	0.20681	0.00489	-2.16172	-0.36449	2.52620	4.75933
29.00000	0.64997	0.00013	0.41670	0.00505	-2.16172	-0.66402	2.82574	4.75933
30.00000	0.80656	0.00014	-0.52364	0.00548	-2.52620	-0.29954	2.82574	3.49239
31.00000	0.67183	0.00013	-0.35033	0.00515	-0.96356	-0.36449	1.32805	4.57262
32.00000	0.80107	0.00015	0.53008	0.00588	-0.96356	-0.66402	1.62759	3.49239
33.00000	0.66734	0.00013	0.14688	0.00537	-1.32805	-0.29954	1.62759	4.57262
34.00000	0.81210	0.00015	-0.73353	0.00589	-0.36449	-0.29954	0.66402	3.49239

**Table 7-7. F380M quads (closure amplitudes and their phases).**

	amp	amperr	phi/deg	phierr/deg
0.00000	0.60767	0.00013	1.43926	0.01054
1.00000	0.69722	0.00015	-7.99574	0.01453
2.00000	1.20244	0.00027	61.82251	0.08987
3.00000	0.98409	0.00021	31.86824	0.05261
4.00000	1.26348	0.00022	-7.57521	0.02612
5.00000	1.19844	0.00029	61.82280	0.08974
6.00000	1.24336	0.00025	32.29485	0.06652
7.00000	1.39235	0.00032	61.87596	0.10406
8.00000	1.45299	0.00032	32.02665	0.07779
9.00000	1.49392	0.00032	32.58274	0.07943
10.00000	1.81239	0.00046	-57.36233	0.15203
11.00000	0.99665	0.00023	12.03956	0.02880
12.00000	1.26358	0.00029	-18.07604	0.06136
13.00000	1.15797	0.00023	12.10636	0.03331
14.00000	1.47660	0.00033	-18.35078	0.07198
15.00000	1.51798	0.00031	-17.79628	0.07395
16.00000	1.16201	0.00028	60.62824	0.09466
17.00000	1.16865	0.00024	30.60334	0.06852
18.00000	1.20153	0.00027	31.16195	0.07003
19.00000	1.02815	0.00021	39.03848	0.04367
20.00000	0.98449	0.00021	-56.83042	0.08248
21.00000	0.54146	0.00014	12.57497	0.01577
22.00000	0.68641	0.00015	-17.54819	0.03342
23.00000	0.66090	0.00015	11.72763	0.01889
24.00000	0.84274	0.00018	-18.72845	0.04079
25.00000	1.19822	0.00024	-17.58859	0.05850
26.00000	1.22080	0.00025	59.71681	0.09927
27.00000	1.22792	0.00021	29.69569	0.07160
28.00000	1.74575	0.00038	30.83418	0.10133
29.00000	1.42183	0.00029	39.62025	0.05983
30.00000	1.06397	0.00025	60.26211	0.08690
31.00000	1.07015	0.00023	30.24255	0.06298
32.00000	0.88224	0.00017	31.36091	0.05157
33.00000	0.82442	0.00015	39.59876	0.03492
34.00000	1.49903	0.00031	39.19522	0.06297

**Table 7-8. F430M quads (closure amplitudes and their phases)**

	amp	amperr	phi/deg	phierr/deg
0.00000	0.65270	0.00012	8.48745	0.01010
1.00000	0.73283	0.00013	-15.63406	0.01407
2.00000	1.17266	0.00023	47.00775	0.06961
3.00000	0.98181	0.00018	11.99675	0.04213
4.00000	1.18698	0.00017	-15.68926	0.02246
5.00000	1.12852	0.00022	47.12534	0.06706
6.00000	1.17310	0.00019	12.35254	0.05053
7.00000	1.31209	0.00026	46.96559	0.07779
8.00000	1.34464	0.00025	12.26747	0.05772
9.00000	1.35908	0.00025	12.44854	0.05840
10.00000	1.61989	0.00034	-56.93433	0.10978
11.00000	0.96245	0.00019	6.09029	0.02525
12.00000	1.19502	0.00023	-29.57471	0.04904
13.00000	1.11900	0.00020	5.92689	0.02859
14.00000	1.36972	0.00028	-29.64949	0.05627
15.00000	1.38424	0.00024	-29.46787	0.05676
16.00000	1.16270	0.00023	40.14437	0.07472
17.00000	1.14623	0.00020	4.80967	0.05333
18.00000	1.15845	0.00022	4.98059	0.05396
19.00000	1.01069	0.00017	26.95296	0.03425
20.00000	0.98025	0.00017	-56.68973	0.06652
21.00000	0.58249	0.00012	6.31547	0.01541
22.00000	0.72321	0.00013	-29.34742	0.02981
23.00000	0.69795	0.00013	5.36505	0.01802
24.00000	0.85430	0.00015	-30.19987	0.03520
25.00000	1.14368	0.00020	-29.51353	0.04742
26.00000	1.19822	0.00021	39.36929	0.07673
27.00000	1.18131	0.00018	4.01600	0.05458
28.00000	1.58139	0.00028	4.71195	0.07318
29.00000	1.33888	0.00023	27.46209	0.04491
30.00000	1.06724	0.00021	38.90148	0.06860
31.00000	1.05207	0.00019	3.53850	0.04905
32.00000	0.88031	0.00014	4.50803	0.04086
33.00000	0.83676	0.00013	27.72450	0.02814
34.00000	1.40826	0.00024	27.90623	0.04697

**Table 7-9. F480M quads (closure amplitudes and their phases)**

	amp	amperr	phi/deg	phierr/deg
0.00000	0.72570	0.00012	6.13146	0.00952
1.00000	0.78904	0.00013	-0.36498	0.01391
2.00000	1.13430	0.00019	53.19968	0.06628
3.00000	0.99063	0.00016	32.43338	0.04216
4.00000	1.13434	0.00016	0.19922	0.01986
5.00000	1.09468	0.00019	53.21296	0.06418
6.00000	1.12491	0.00017	33.10905	0.04803
7.00000	1.24002	0.00021	53.35660	0.07244
8.00000	1.24890	0.00022	32.37008	0.05339
9.00000	1.27263	0.00020	33.04635	0.05429
10.00000	1.43769	0.00025	-33.53083	0.08822
11.00000	0.96517	0.00017	20.22176	0.02137
12.00000	1.13559	0.00019	-0.55432	0.04046
13.00000	1.09320	0.00017	20.37535	0.02373
14.00000	1.26080	0.00023	-1.29138	0.04505
15.00000	1.28468	0.00020	-0.62475	0.04561
16.00000	1.13275	0.00020	47.31183	0.07045
17.00000	1.11022	0.00018	26.31284	0.05039
18.00000	1.13135	0.00018	26.98785	0.05125
19.00000	1.01906	0.00016	32.69476	0.03322
20.00000	0.98407	0.00015	-32.92121	0.06045
21.00000	0.66059	0.00013	20.83078	0.01476
22.00000	0.77731	0.00012	0.04700	0.02781
23.00000	0.76423	0.00013	21.07791	0.01674
24.00000	0.88139	0.00015	-0.59238	0.03156
25.00000	1.10838	0.00017	-0.40538	0.03985
26.00000	1.15689	0.00019	47.39913	0.07176
27.00000	1.13391	0.00017	26.42048	0.05121
28.00000	1.42607	0.00023	26.60132	0.06432
29.00000	1.25766	0.00021	32.21085	0.04074
30.00000	1.06399	0.00020	47.16623	0.06628
31.00000	1.04286	0.00018	26.17028	0.04751
32.00000	0.91234	0.00013	27.12622	0.04118
33.00000	0.87487	0.00013	32.97671	0.02821
34.00000	1.30323	0.00022	32.41332	0.04219